Arch. Metall. Mater. **67** (2022), 4, 1293-1298

DOI: https://doi.org/10.24425/amm.2022.141054

BINGGE ZHAO[1,2], YUANFANG WANG[1,2], CHENYU SUN[1,2], KAI DING[1,2*], GUANZHI WU[1,2], TAO WEI[1,2], HUA PAN[3,4*], YULAI GAO[1,2*]

EFFECT OF HIGH-TEMPERATURE ANNEALING ON THE CROSS-TENSION PROPERTY OF RESISTANCE SPOT WELDED MEDIUM-Mn STEEL

As one of the most promising 3rd generation advanced high strength steels (AHSS), medium Mn steels attract much attention because of their exceptional mechanical property and reasonable cost. However, their application in the modern automotive industry is limited by poor weldability. In this study, 7Mn steel was welded by resistance spot welding (RSW), which was followed by high-temperature annealing to increase the cross-tension property. With this effort, enhanced cross-tension strength (CTS) with a partial interfacial fracture (PIF) mode was realized. During the annealing after RSW that produced martensite, austenitization was realized and then evolved into martensite by the following air cooling. This process produced structure homogeneity across the joint. With respect to the RSW joint, martensite remained the dominant structure after annealing while the diffusion of C and Mn solutes was triggered. With the increase of annealing temperature, the diffusion was enhanced, and the grain boundary embrittlement was reduced, leading to higher CTS.

Keywords: medium Mn steel; resistance spot welding; cross-tension strength; martensite; fracture

1. Introduction

Welding is an important approach to join steel sheets. Resistance spot welding (RSW) possesses high welding speed and suitability for robotization [1]. As a result, it is widely used in body-in-white manufacture, e.g. 2,000-5,000 spot joints are usually contained in a modern vehicle. However, the welding can exert melting and rapid solidification that produces non-equilibrium phases [2], which may erase the designed structure of the steel sheet and deteriorate the corresponding mechanical properties of the steel. Consequently, it is important to develop an accessible approach to tailor the structure of the RSW joints to improve their mechanical properties.

Advanced high strength steels (AHSS) are attracting more and more attention attributing to the increasing requirements of safety, vehicle performance, and energy economy in the automotive industry. Compared with conventional steels, AHSS has enhanced mechanical properties and higher formability [3,4]. Among the three generations of AHSS, the 1st generation AHSS contains multiple phases with improving strength and working hardening [5] while the 2nd generation AHSS has outstanding strength and elongation simultaneously [6]. However, they are limited in processing accessibility and high cost. As a result, the 3rd generation AHSS was developed, by which satisfying trade-off between strength and ductility but the lower cost is facilitated [7,8]. Medium Mn steels, a typical 3rd generation AHSS, are considered as the most promising candidate in the automotive industry attributing to their exceptional property with reasonable cost [9-12]. However, it is still a challenge to improve the weldability of medium Mn steel because of the evident tendency for the element Mn to segregate in the centerline of the nugget. The increase of cross-tension strength (CTS), an essential parameter to characterize the weldability of steel sheets [13], remains challenged in medium Mn steels. Park et al. have obtained a CTS of 1.4 kN in the joints of medium Mn steel [14]. Compared with other steels, this value is rather low and cannot meet the requirement of automotive manufacturing [15]. In Wang's study, in situ post welding pulses were adopted and played the role of annealing, by which the CTS was increased [16]. Li has created a novel shim-assisted RSW method to increase the CTS as much

[1] SHANGHAI UNIVERSITY, STATE KEY LABORATORY OF ADVANCED SPECIAL STEEL AND SHANGHAI KEY LABORATORY OF ADVANCED FERROMETALLURGY, 200444, P.R. CHINA
[2] SHANGHAI UNIVERSITY, SCHOOL OF MATERIALS SCIENCE AND ENGINEERING, CENTER FOR ADVANCED SOLIDIFICATION TECHNOLOGY (CAST), SHANGHAI, 200444, P.R. CHINA
[3] STATE KEY LABORATORY OF DEVELOPMENT AND APPLICATION TECHNOLOGY OF AUTOMOTIVE STEELS, SHANGHAI 201900, P.R. CHINA
[4] AUTOMOBILE STEEL RESEARCH INSTITUTE, R&D CENTER, BAOSHAN IRON & STEEL CO., LTD. SHANGHAI 201900, P.R. CHINA

* Corresponding authors: dingkaiwsj@shu.edu.cn; hpan@baosteel.com; ylgao@shu.edu.cn

as possible. Meanwhile, the nugget pull-out fracture rather than interfacial fracture was obtained, suggesting the outstanding ductility with this method [17].

In this study, high-temperature annealing at different temperatures was applied to enhance the cross-tension property of 7Mn RSW joints, and the relation between the cross-tension property and microstructure was demonstrated.

2. Materials and methods

2.1. Materials

Uncoated cold-rolled 7Mn steel sheets with a thickness of 1.4 mm were welded by resistance spot welding. The chemical composition of the steel is listed in TABLE 1.

TABLE 1

Chemical composition of the 7Mn steel (wt.%)

C	Mn	Si	Al	S	P	Fe
0.13	6.98	0.22	0.03	0.005	0.006	Bal.

2.2. Resistance spot welding

7Mn steels were joined by resistance spot welding, which was realized by a medium frequency direct current machine (DM-150, Shanghai Medar) using an electrode with a face diameter of 6 mm. Two 7Mn steel sheets with the dimensions of $150 \times 50 \times 1.4$ mm^3 were welded according to the RSW protocol shown in Fig. 1. Two current pulses of 8.6 kA and 100 ms were applied to the 7Mn sheet with an interval of 20 ms. The joints were cooled down to room temperature and hold for 400 ms, which was followed by a current of 3.4 kA and duration of 100 ms, respectively, to temper the joints. The specimens are then cooled down to room temperature. The electrode force during the welding and tempering was 5.5 kN, hindering the formation of shrinkage porosities during the solidification process as much as possible.

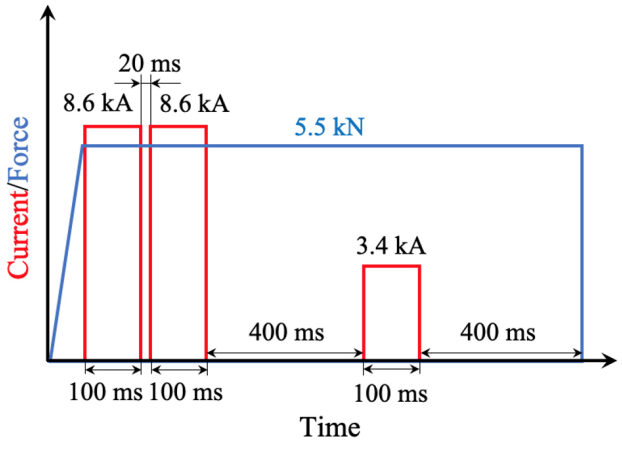

Fig. 1. Schematic of the RSW protocol

2.3. Post-weld heat treatment

After RSW, post-weld annealing was applied to the joints to improve the CTS. The RSW joints were heated to 800, 810, 820, and 830°C and annealed for 7 min, respectively. After that, the specimens were cooled in the air for cross-tension test and structure characterization.

2.4. Mechanical tests

The RSW specimens with PWHT were subjected to a cross-tension test by using an electromechanical testing system (Instron 5581) at a crosshead speed of 10 mm/min at room temperature. With the aid of a built-in extensometer, the load and displacement data were directly obtained from the testing system. The cross-tension strength was obtained from the peak point in the load-displacement curve. The microhardness of the RSW nugget was measured by a Vickers microhardness tester (MH-5L) with an indentation load of 500 gf for a hold time of 15 s.

2.5. Microstructure characterization

The fracture morphology and microstructure of RSW specimens were observed by optical microscopy (OM, Imager A2m, Zeiss) and scanning electron microscopy (SEM, VEGA 3 SBH-Easy Probe, TESCAN). Metallographic images were obtained by etching the specimens with a saturated picric acid solution. The distribution of elements in the nugget was acquired by an electron probe microanalyzer (EPMA, 8050G, SHIMADZU). X-ray diffraction (XRD, Bruker D8 ADVANCE DAVINCI) was used to identify the phase constitution of the RSW joint.

3. Results and discussion

To reveal the effect of annealing on the joint, metallographic images of the RSW joints after annealing at different temperatures are exhibited in Fig. 2. It has been stated that a RSW joint usually consists of nugget, heat-affected zone (HAZ), and BM [18,19]. In the current study, however, these zones are hardly to be distinguished by these metallographic images. Moreover, the joints with different annealing heat treatments display similar structure, as evidenced by Fig. 2(a)-(d). Compared with optical microscopy, the microhardness distribution is associated with the structure of a joint. Fig. 2(e) presents the microhardness across the nugget. Despite the different annealing temperatures, all specimens possess similar microhardness. This is in agreement with the metallographic images. For the RSW joints, the nugget, HAZ, and BM experience different thermal histories and therefore possess various structural zones. Whereas they are annealed simultaneously, similar phase transformation occurs in the nugget, contributing to the similar structure and microhardness.

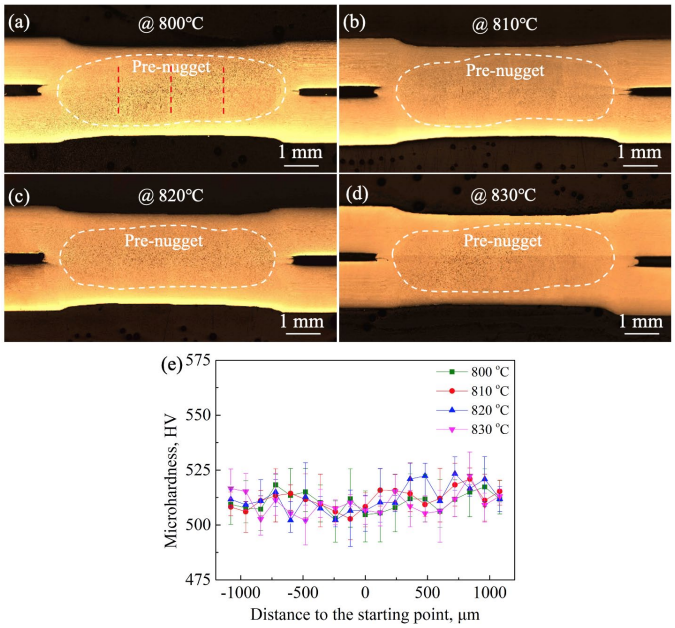

Fig. 2. Metallographic images and microhardness distribution of the RSW nugget after annealing at (a) 800°C, (b) 810°C, (c) 820°C, and (d) 830°C. The nugget after annealing cannot be clearly distinguished. Based on our experience, the RSW process is stable, and the nugget size of different specimens keeps similar. As a result, the nugget size with RSW can be used to determine the boundary between the nugget and HAZ of the joint with high-temperature annealing. To differ the case after RSW, pre-nugget is used here to denote the nugget area after annealing. (e) Vickers microhardness of the nugget along the thickness direction. The microhardness indentations are marked by dashed lines in (a)

Fig. 3 is the XRD pattern of the RSW joint with annealing at 800°C. Generally, to identify the phase constitution after rapid quenching, the lattice parameters should be calculated [20-22]. But for medium Mn steels, their phase transitions have been well recognized. It has to note that the joint is mainly dominated by martensite (PDF no. 44-1292) with some residual austenite (PDF no. 52-0512). 7Mn steel contains relatively high alloying elements, and its hardenability can be significantly enhanced.

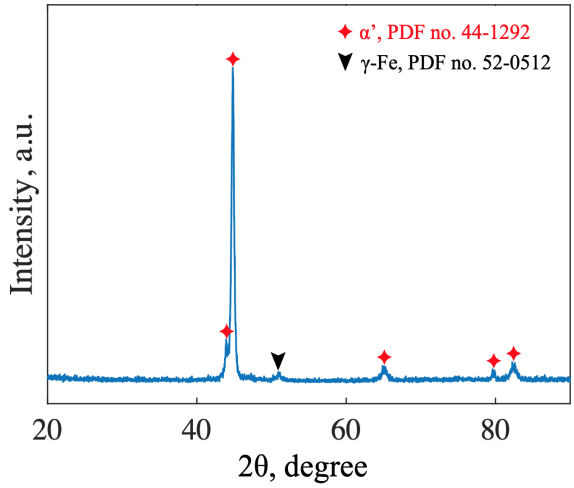

Fig. 3. XRD pattern of the RSW joint with annealing at 800°C. It is composited of martensite with a little residual austenite

As a result, even the air cooling after annealing facilitates the formation of martensite. Other RSW joints experience similar cooling process and possess martensite as well.

It has been reported that the nugget structure is mainly responsible for the cross-tension property of the RSW joints [23]. Fig. 4 shows the details of the nugget structure of the RSW joints annealed at different temperatures. Similar with our previous studies [16,24], the nugget is mainly composed of columnar grains attributing to the rapid heat transfer along the thickness direction during the RSW process. It has been reported that solute segregation can easily occur in a directionally solidified alloy [25,26]. In this study, both C and Mn in 7Mn steel are prone to segregating to the nugget centerline due to their equilibrium segregation coefficient smaller than 1.0 [27], which can deteriorate the bonding force between the upper and bottom steel sheet. Such segregation has been demonstrated in our recent results. During the following annealing after RSW,

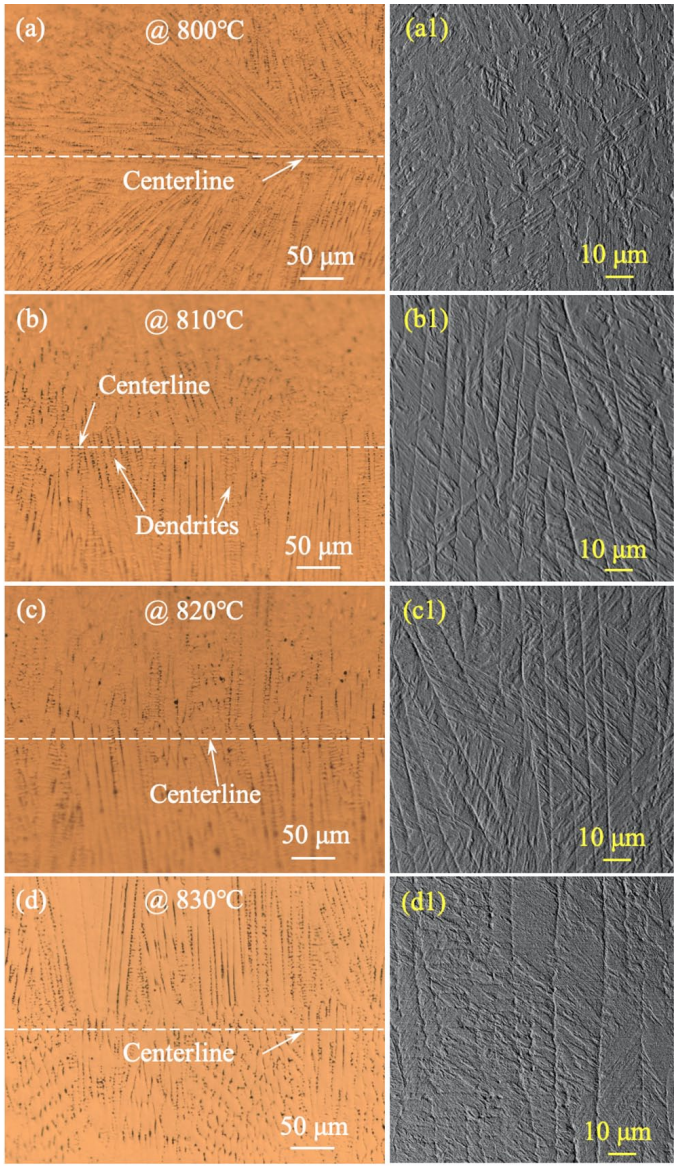

Fig. 4. The nugget structure of RSW welds with different annealing temperatures: (a)-(d) Metallographic images of the nugget. (a1)-(d1) Secondary electron images of the nugget

austenite forms from martensite, which exerts an obvious effect on the CTS of RSW joints.

Fig. 5 displays the cross-tension results of RSW 7Mn steel. Fig. 5(a)-(d) are the load-displacement curves after high-temperature annealing at 800, 810, 820, and 830°C, respectively. CTS is estimated by the highest point in the load-displacement curve. Under each condition, three specimens were tested to demonstrate the reproducibility of the welding. The average CTS with 95% confidence interval at different annealing temperatures is summarized in Fig. 5(e). With the annealing temperature increasing from 800 to 830°C, higher CTS is obtained. Compared with the RSW joint of 7Mn steel with CTS of 1.8 kN [16,24], the CTS after high-temperature annealing stands at 3.0 kN, namely the improvement of CTS is as high as 66.7%. It has to note that the CTS with different annealing temperatures overlaps with each other, and the analysis of variance (ANOVA) method suggests the average CTS is not significantly different at 95% confidence interval. However, this phenomenon cannot be attributed to the errors in statistics because the overall increase of CTS is rather limited with the annealing temperature increasing from 800°C to 830°C. The increase of annealing temperature can enhance the diffusion of C and Mn, which reduces the segregation along the nugget centerline and leads to a higher CTS. As mentioned above, severe segregation of C and Mn is deemed to occur in the RSW 7Mn steel, causing the grain boundary embrittlement

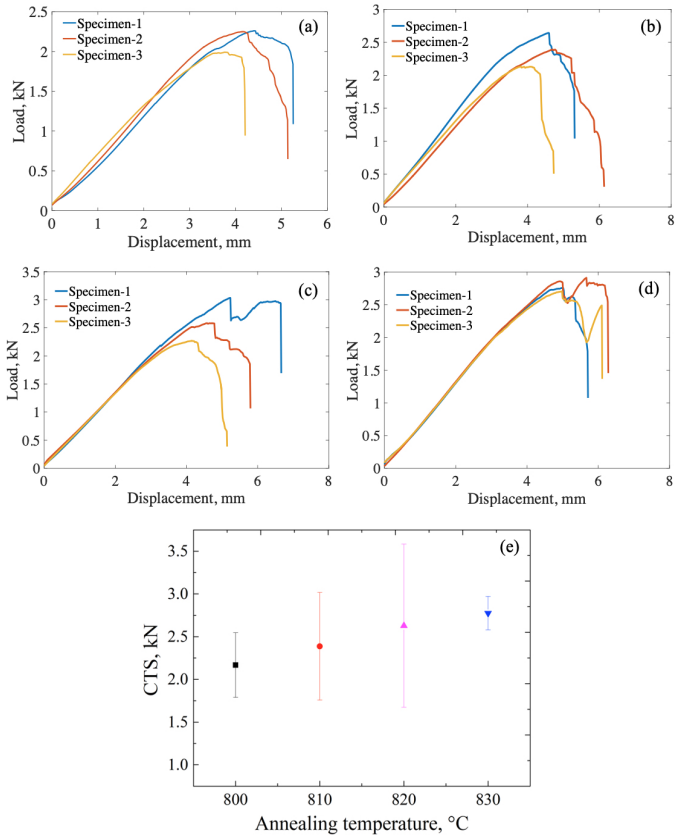

Fig. 5. Cross-tension results of the 7Mn RSW joints with high-temperature annealing at different temperatures: (a)-(d) Load-displacement curves of the specimens with annealing temperatures of 800, 810, 820, and 830°C. respectively. (e) The mean CTS with 95% confidence interval versus annealing temperature

and deteriorating the bonding force [12]. With the annealing at austenitization zone, the transition from martensite to austenite occurs, which is dominated by the diffusion of C and Mn [12,28]. In other words, the diffusion of C and Mn is accelerated, which can reduce the segregation along the nugget centerline. Fig. 6 displays the EPMA mapping results along the centerline of the nugget experiencing different annealing treatments. Our previous study has demonstrated the serious segregation of C and Mn along the nugget centerline [29]. Although the segregation of C and Mn along the lath boundaries cannot be completely diminished, the segregation along the centerline nearly vanishes. This can enhance the bonding force between the upper and bottom steel sheets, causing a higher CTS. In other words, the segregation of C and Mn is indeed reduced, which produces a higher CTS with the increase of annealing temperature rather than being caused by statical errors. It has to note that Mn cannot completely dissolve in the martensite matrix, and thus only limited increase of CTS is obtained in this work. The diffusion is improved at higher annealing temperature, leading to a higher CTS.

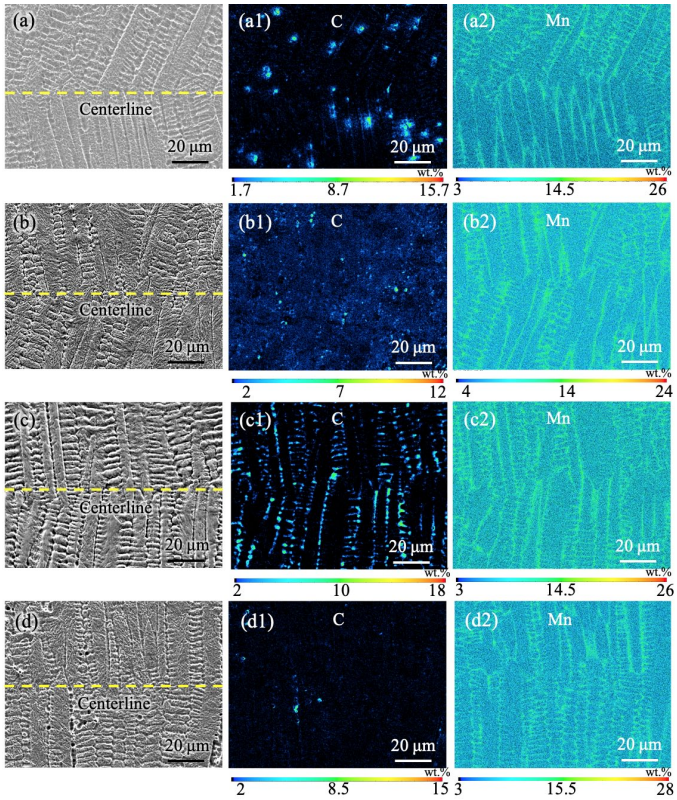

Fig. 6. EPMA results of the RSW joints with annealing at different temperatures: (a)-(d) The morphology near the centerline of the nugget with annealing at 800, 810, 820, and 830°C, respectively. (a1)-(d1) The distribution of C near the centerline of the nugget with annealing at 800, 810, 820, and 830°C, respectively. (a2)-(d2) The distribution of Mn near the centerline of the nugget with annealing at 800, 810, 820, and 830°C, respectively

After the cross-tension test, the fractured joints were observed by optical microscopy. The results are exhibited in Fig. 7. It is noted that both the broken nugget and base metal (BM) are

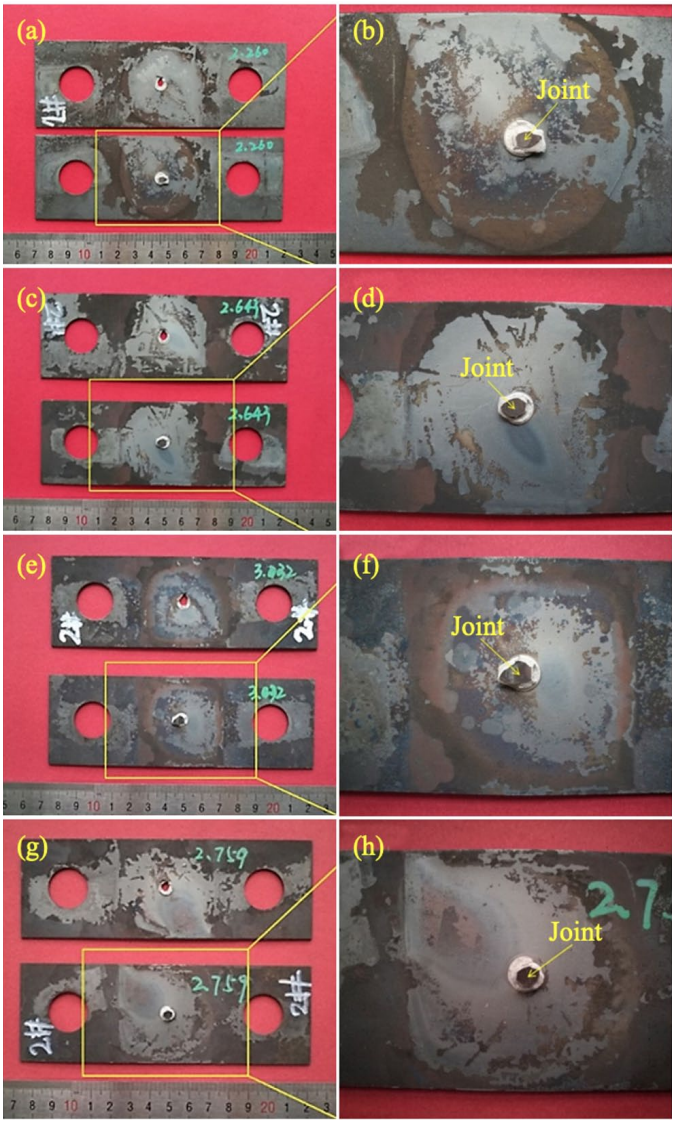

Fig. 7. Fracture morphology of the 7Mn welds after the cross-tension test: (a) and (b) are fractured sheets and joint after annealing at 800°C. (c) and (d) are fractured sheets and joint after annealing at 810°C. (e) and (f) are fractured sheets and joint after annealing at 820°C. (g) and (h) are fractured sheets and joint after annealing at 830°C

observed in the fractured joint, suggesting the 7Mn joints fail in a partial interfacial fracture (PIF) mode. Despite the increase of annealing temperature and CTS, plastic deformation is less involved during the cross-tension test.

The fracture morphology of the 7Mn joints after the cross-tension test is further characterized by SEM, and the results are displayed in Fig. 8. The overview of the fracture is listed in Fig. 8(a)-(d). Clearly, part of the nugget stays with the BM of the other steel sheet. This is in agreement with the optical images shown in Fig. 7, which evidences the PIF mode. The fracture details of each specimen are also explored by SEM. Zone A reflects the structure of the BM. For all specimens, some dimples are observed in zone A. During the cross-tension tests, bending deformation occurs initially but the specimen finally fails in a shear load [13]. The dimples in the BM suggest the plastic deformation of RSW joints at the last stage of the cross-tension test in a shear load. Meanwhile, the intergranular fracture is observed in the specimen with the annealing temperature of 800°C (Fig. 8(a1)), implying a higher fraction of brittle deformation under this condition. As indicated in Fig. 5, joints with the annealing temperature of 800°C possess the lowest CTS and displacement, which is ascribed to the brittle fracture.

Zones B and C reflect the structure details of the nugget. Columnar grains are observed from the overview sight. This is caused by the strong heat conduction along the thickness direction [30]. As typically indicated in Fig. 8(c3) and (d3), the intergranular fracture is detected. Despite the occasional dimples (Fig. 8(d2)), intergranular fracture dominates the nugget, implying the brittle fracture is the main failure mechanism. During the cross-tension test, cracks initiate at the faying interface of the steel sheets and then propagate along the centerline of the nugget. Since the embrittlement caused by the segregation of C and Mn is reduced by the annealing, cracks deflect to the thickness direction rather than along the centerline direction and propagate in the BM. Compared with the nugget, only solid-state transformation occurs in the BM on the annealing and following air cooling. Under this condition, the segregation of C and Mn is hindered, and plastic deformation becomes the dominant failure mechanism, producing a higher CTS.

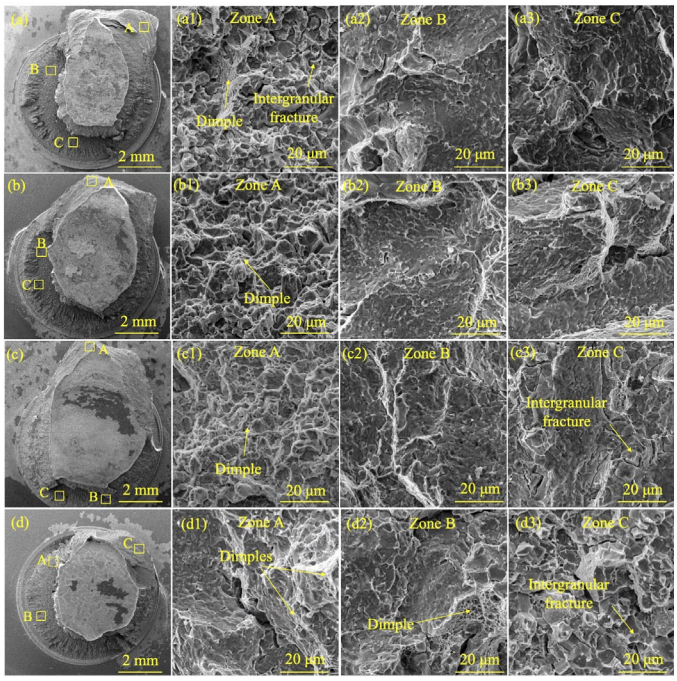

Fig. 8. SEM images showing the cross-tension fracture of RSW 7Mn welds with different annealing temperatures: (a)-(d) The overview of the fracture of 7Mn weld with annealing temperatures of 800, 810, 820, and 830°C, respectively. Details of zones A, B, and C are displayed in images (a1)-(d3)

4. Conclusions

In this study, 7Mn steel sheets were joined by resistance spot welding. By additional post-weld annealing, the cross-tension property of the welds was enhanced. Based on the structure

characterization and microhardness distribution, the following conclusions are obtained.

(1) Relatively high alloying content is contained in 7Mn steel, which facilitates the formation of martensite even by air cooling.

(2) With the post-weld annealing at the temperature of 800, 810, 820, and 830°C, structure heterogeneity in the nugget, HAZ and BM is diminished, producing martensite across the joint. With the high-temperature annealing, the joints fail in a partial interfacial fracture (PIF) mode.

(3) Although the room-temperature structure of the joint cannot be changed by the high-temperature annealing, the segregation of C and Mn along the nugget centerline is reduced, which enhances the bonding force of the steel sheet and leads to higher CTS. The reduction of C and Mn segregation is enhanced with the annealing temperature increasing from 800°C to 830°C, facilitating the monotonous increase of CTS.

Acknowledgements

This work was supported by the National Natural Science Foundation of China (Grant no. U1760102), Independent Research Project of State Key Laboratory of Advanced Special Steel and Shanghai Key Laboratory of Advanced Ferrometallurgy (Shanghai University, Grant no. 19DZ2270200), the State Key Laboratory of Development and Application Technology of Automotive Steels (Baosteel Group, Grant no. Y17ECEQ05Y).

Declaration of interest statement

The authors declare no conflict of interest.

REFERENCES

[1] H. Eisazadeh, M. Hamedi, A. Halvaee, Mater. Des. **31**, 149 (2010).

[2] Y. Gao, B. Zhao, J.J. Vlassak, C. Schick, Prog. Mater. Sci. **104**, 53 (2019).

[3] C. Lesch, N. Kwiaton, F.B. Klose, Steel Res. Int. **88**, 1700210 (2017).

[4] R. Kuziak, R. Kawalla, S. Waengler, Arch. Civ. Mech. Eng. **8**, 103 (2008).

[5] H. Aydin, E. Essadiqi, I.-H. Jung, S. Yue, Mater. Sci. Eng. A **564**, 501 (2013).

[6] V. Shterner, A. Molotnikov, I. Timokhina, Y. Estrin, H. Beladi, Mater. Sci. Eng. A **613**, 224 (2014).

[7] S. Chen, R. Rana, A. Haldar, R.K. Ray, Prog. Mater. Sci. **89**, 345 (2017).

[8] D.Q. Zou, S.H. Li, J. He, B. Gu, Y.F. Li, Mater. Sci. Eng. A **715**, 243 (2018).

[9] Y.K. Lee J. Han, Mater. Sci. Technol. **31**, 843 (2015).

[10] Y. Chang, C.Y. Wang, K.M. Zhao, H. Dong, J.W. Yan, Mater. Des. **94**, 424 (2016).

[11] Y. Li, W. Li, W. Liu, X. Wang, X. Hua, H. Liu, X. Jin, Acta Mater. **146**, 126 (2018).

[12] M. Kuzmina, D. Ponge, D. Raabe, Acta Mater. **86**, 182 (2015).

[13] Y.J. Chao, J. Eng. Mater. Technol. **125**, 125 (2003).

[14] G. Park, K. Kim, S. Uhm, C. Lee, Mater. Sci. Eng. A **752**, 206 (2019).

[15] D.C. Saha, Y. Cho, Y.-D. Park, Sci. Technol. Weld. Joining **18**, 711 (2013).

[16] Y. Wang, K. Ding, B. Zhao, Y. Zhang, G. Wu, T. Wei, H. Pan, Y. Gao, Highly Enhanced Cross Tensile Strength of the Resistance Spot Welded Medium Manganese Steel by Optimized Post-Heating Pulse, TMS 2020 149th Annual Meeting & Exhibition Supplemental Proceedings, 2020, pp. 1871–1880.

[17] S. Li, S. Yang, Q. Lu, H. Luo, W. Tao, Metall. and Mater. Trans. B **50**, 1 (2019).

[18] D.C. Saha, S. Han, K.G. Chin, I. Choi, Y.D. Park, Steel Res. Int. **83**, 352 (2012).

[19] D. Shirmohammadi, M. Movahedi, M. Pouranvari, Mater. Sci. Eng. A **703**, 154 (2017).

[20] L. Cheng, A. Böttger, Th.H. de Keijser, E. J. Mittemeijer, Scr. Metall. Mater. **24**, 509 (1990).

[21] H. Xiao, S. Zheng, Y. Xin, J. Xu, K. Han, H. Li, Q. Zhai, Metals **10**, 8 (2020).

[22] S. Kajiwara, S. Uehara, Y. Nakamura, Philos. Mag. Lett. **60**, 147 (1989).

[23] M. Stadler, M. Gruber, R. Schnitzer, C. Hofer, Weld. World **64**, 335 (2020).

[24] Y. Wang, K. Ding, B. Zhao, Y. Zhang, G. Wu, T. Wei, H. Pan, Y. Gao, Effect of the Cooling Time on the Cross Tensile Strength of the Resistance Spot Welded Medium Manganese Steel, TMS 2020 149th Annual Meeting & Exhibition Supplemental Proceedings, pp. 515–523, 2020.

[25] R. Trivedi, S. Liu, P. Mazumder, E. Simsek, Sci. Technol. Adv. Mater. **2**, 309 (2001).

[26] W. Du, C. Song, F. Zhang, M. Jiang, Q. Zhai, K. Han, Metall. Mater. Trans. B **46**, 2423 (2015).

[27] V.P. Kujanpää, S.A. David, ICALEO **1986**, 63 (1986).

[28] N. Nakada, K. Mizutani, T. Tsuchiyama, S. Takaki, Acta Mater. **65**, 251 (2014).

[29] B. Zhao, Y. Wang, K. Ding, G. Wu, T. Wei, H. Pan, Y. Gao, J. Mater. Eng. Perform, **30**, 1259 (2021).

[30] P.S. Wei,T.H. Wu, Int. J. Heat Mass Transfer **79**, 408 (2014).